INSTITUTE OF PHYSICS PUBLISHING SUPERCONDUCTOR SCIENCE AND TECHNOLOGY
Supercond. Sci. Technol. **17** (2004) 51–57 PII: S0953-2048(04)66338-X

Temperature rise in an Sm-based bulk superconductor after applying iterative pulse fields

Hiroyuki Fujishiro[1], **Kazuya Yokoyama**[2], **Tetsuo Oka**[2] **and Koshichi Noto**[1]

[1] Faculty of Engineering, Iwate University, 4-3-5 Ueda, Morioka 020-8551, Japan
[2] Iwate Industrial Promotion Center, 3-52-2, Iioka-shinden, Morioka 020-0852, Japan

E-mail: fujishiro@iwate-u.ac.jp

Received 8 July 2003
Published 19 November 2003
Online at stacks.iop.org/SUST/17/51 (DOI: 10.1088/0953-2048/17/1/009)

Abstract
The time evolutions and spatial distributions of temperature rise $\Delta T(t)$ have been measured on the surface of a cryo-cooled SmBaCuO bulk superconductor after iterative pulse field magnetizing with the same amplitude. For the applied pulse field $B_{ex} \leqslant 4.64$ T, the maximum temperature rise ΔT_{max} monotonically decreases and approaches a steady $\Delta T(t)$ behaviour with an increasing number of times of pulse applications. On the other hand, for $B_{ex} = 5.42$ T, ΔT_{max} keeps on increasing after the third pulse application in a specific growth sector region and a clear anisotropic $\Delta T(t)$ behaviour has been found. The magnetic fluxes preferentially enter and leave the bulk superconductor through this sector region. The $\Delta T(t)$ behaviours are closely correlated with the distribution of the trapped field ${B_T}^P$ and can be understood on the basis of the heat generation caused by the flux motion.

1. Introduction

Various kinds of practical applications using the melt-processed REBaCuO superconductors (RE: rare earth ions) have been proposed and developed, e.g., magnetic bearings, levitation systems, high-strength bulk magnets and so on [1]. For applicational purpose, the pulse-field magnetizing (PFM) is a useful method as well as the static field cooled magnetizing (FCM). An improved PFM based on a series of iterative magnetizing operations with sequentially reduced pulse field amplitudes, called the IMRA method, has been proposed [2] and the YBaCuO bulk was reported to trap almost an equal amount of the magnetic flux as that of the FCM in liquid nitrogen [3]. However, at lower temperatures, the maximum trapped magnetic flux by PFM is generally lower than that by FCM even using the IMRA method [4]. The cause has been considered to be the temperature rise due to the dynamical motion of the magnetic fluxes, resulting in the decrease of the pinning force F_p. Yanagi *et al* measured the temperature rise ΔT on the surface of the SmBaCuO bulk after applying the pulse fields [5]. ΔT increased with increasing amplitude of the pulse field, which was as high as 15 K for the pulse field $B_{ex} = 4.7$ T at 42 K. However, there have not been systematic experimental studies on the temperature rise and the trapped field.

We investigated the time evolution and spatial distribution of the temperature rise $\Delta T(t)$ on the surface of the cryo-cooled YBaCuO bulk superconductor after applying the pulse fields by the IMRA technique [6]. We obtained the following conclusions: (i) the maximum temperature rise ΔT_{max} after applying the pulse field increases with increasing the pulse field strength and a larger temperature rise occurs just before the magnetic flux is trapped in the vicinity of the centre of the bulk. (ii) The trapped field ${B_T}^P$ by PFM cannot exceed the trapped field ${B_T}^{FC}$ by FCM operated at the maximum temperature T_{max} through the PFM operation. (iii) $\Delta T(t)$ depends on the position on the bulk surface; the magnetic fluxes move more easily through the growth sector regions (GSRs) than along the growth sector boundaries (GSBs). (iv) $\Delta T(t)$ firstly occurs at the circumference region of the bulk disk and then heat propagates to the centre. These results could well explain the distribution of ${B_T}^P$. The *in situ* temperature monitor on the bulk surface offered valuable information about the magnetizing mechanism in the bulk superconductors.

However, it is difficult to analyse the mechanism of the flux trapping for a series of iterative magnetizing operations such as the IMRA method because the magnitude and the distribution of $B_T{}^P$ is different at the stages before the application of each pulse field. It is desirable to investigate $B_T{}^P$ and $\Delta T(t)$ under a simpler PFM operation. One possible scheme is to use a single magnetic pulse application with various amplitudes, where we can obtain the results under an identical initial condition of no already trapped flux. Another is to use the iterative pulse applications with fixed amplitude, where we can obtain the effect of the pure superposition of pulse fields. The experimental results for both cases may be valuable to analyse the PFM mechanism.

In this paper, we investigate the time and position dependence of the temperature rise $\Delta T(t)$ after PFM for the cryo-cooled SmBaCuO bulk superconductor. The five pulse fields (nos 1–5) with the same amplitude ($B_{ex} = 2.32$–5.42 T) are applied and the relation between $\Delta T(t)$ and $B_T{}^P$ is investigated.

2. Experimental details

The SmBaCuO bulk superconductor of disk shape used in this study was a highly *c*-axis oriented crystal fabricated by Dowa Mining Co, Ltd, which consisted of four growth sectors (GSR1–GSR4). The crystal was composed of $SmBa_2Cu_3O_y$ (Sm123) and Sm_2BaCuO_5 (Sm211) with the molar ratio of Sm123:Sm211 = 1.0:0.3, 15.0wt% Ag_2O powder and 0.5wt% Pt powder. The detailed procedure of the melt growth has been described elsewhere [7]. The initial size of the bulk disk is 46 mm in diameter and 15 mm in thickness. The bulk was uniformly impregnated by epoxy resin in vacuum. The epoxy resin layer on both upper and lower sides of the bulk was removed in order to measure the precise temperature on the bulk surface and to reduce the thermal contact resistance between the bulk and the cold stage. Figure 1 shows the setup of the bulk to a Gifford McMahon (GM) cycle helium refrigerator (AISIN, GR103). The bulk was tightly stuck on the sapphire plate on the cold stage by the insertion of an indium foil. The initial temperature T_s of the bulk surface was $\simeq$38 K. The temperature $T0$ at the centre of the bulk (P0) and the temperatures, $T1$–$T4$, at P1–P4 in the four GSRs were measured using a Teflon-coated chromel-constantan thermocouples (76 μm in diameter) adhered to the bulk surface using GE7031 varnish. P1, P2, P3 and P4 were situated on the centre lines of each GSR with a 9 mm distance from P0. Each temperature was measured about seven times per second just after applying the pulse field.

The bulk crystal was magnetized using a pulse coil dipped in liquid N_2. The rise time of the pulse field B_{ex} was about $\sim$10 ms. The strength of B_{ex} was calculated from the current flowing through the coil, which ranged from 2.32 T to 5.42 T. Five magnetic pulses with the same amplitude were applied sequentially and $\Delta T(t)$ and $B_T{}^P$ were measured at each stage. The Hall sensor (F W Bell, model BHT 921) was adhered to the position PH with a 2.5 mm distance from P0 as shown in figure 1, which monitored the trapped magnetic field $B_T{}^P$ just on the bulk. The two-dimensional distribution of the trapped magnetic field $B_T{}^{3\,mm}$ was monitored at each stage using an axial-type Hall sensor, which scanned 3 mm above the bulk surface stepwise with a pitch 1.2 mm. The $B_T{}^{3\,mm}$ values at P0–P4 ($B_T{}^{3\,mm}0$–$B_T{}^{3mm}4$) were extracted from the distribution. The trapped field $B_T{}^{FC}$ by FCM was also measured at several temperatures using the cryo-cooled superconducting magnet. During FCM, the static magnetic field of 5 T was decreased down to 0 T in 18 min (0.278 T min^{-1}).

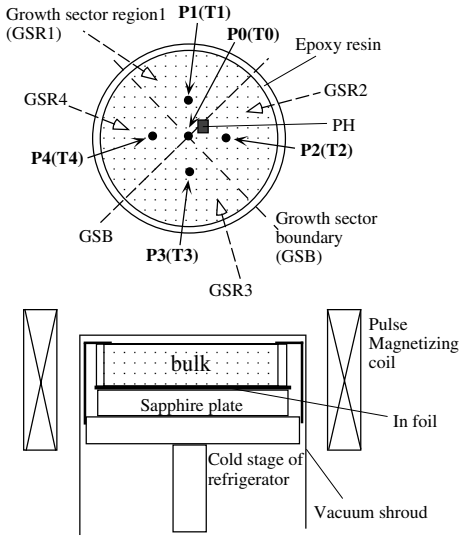

Figure 1. The experimental setup of the SmBaCuO bulk superconductor for the temperature measurements. The setting of the bulk in the Gifford McMahon (GM) cycle helium refrigerator is shown. The positions P0–P4 for the temperature measurement of $T0$–$T4$ are indicated. The trapped fields $B_T{}^{3\,mm}0$–$B_T{}^{3\,mm}4$ are also measured at 3 mm above the P0–P4. The trapped field $B_T{}^P$ is measured using a Hall sensor fixed at the position PH.

3. Results and discussion

Figures 2(*a*)–(*e*) summarize the results of the first (no 1) pulse application. Figures 2(*a*)–(*c*) show the time evolutions of the temperatures at the five positions after applying the pulse of $B_{ex} = 2.32$ T, 3.01 T and 3.87 T, respectively. We define the rise time $t(60\%)$ to reach 60% of the maximum temperature rise ΔT_{max}, which is presented in the insets of each figure. Figure 2(*d*) shows the $B_T{}^{3\,mm}$ after each pulse for respective positions.

In figure 2(*a*) for $B_{ex} = 2.32$ T, the maximum temperature rise ΔT_{max} is only about 4 K and almost independent of the measuring points. The $t(60\%)$ values of $T1$–$T4$ are about 2 s and also nearly independent of the measuring positions. The $t(60\%)$ value of $T0$, however, is almost 4 s and about two times as long as those of $T1$–$T4$. The rise time of $T(t)$ at a measuring point is determined by the thermal diffusivity $\alpha(T)$ and the distance from the heat source [8]. The $T(t)$ results indicate that the heat is generated in the peripheral region of the bulk and diffuses towards the central region. In figure 2(*d*), the trapped field $B_T{}^{3\,mm}$ monitored 3 mm above each point is below 0.1 T for $B_{ex} = 2.32$ T at all the measuring points, which suggests that the intrusion of the magnetic flux is inhibited by the surface barriers. For $B_{ex} = 2.32$ T, the heat generation actually occurs just at the surface on the circumference of the bulk disk.

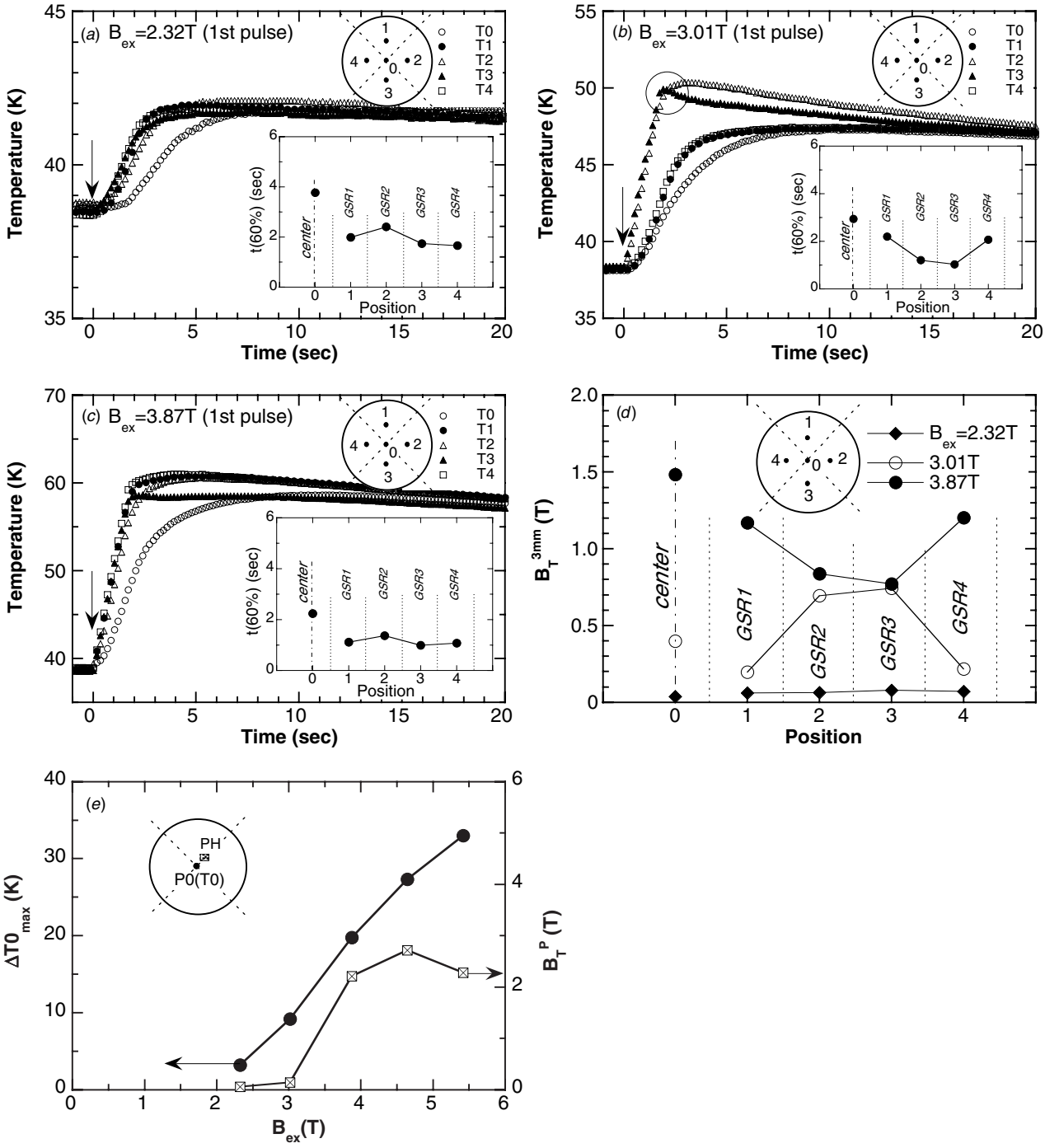

Figure 2. The time evolution of the temperatures $T0(t)$–$T4(t)$ after applying the first pulse field of (*a*) $B_{ex} = 2.32$ T, (*b*) 3.01 T and (*c*) 3.87 T, respectively. The circle in (*b*) indicates the shoulder-like anomaly in $T3(t)$. The rise time $t(60\%)$ to reach 60% of the maximum temperature ΔT_{max} is presented in the insets of each figure. (*d*) The $B_T{}^{3\,mm}$ values at P0–P4 after each pulse. (*e*) $\Delta T0_{max}$ and $B_T{}^{P}$ as a function of B_{ex} after the first pulse.

In figure 2(*b*) for $B_{ex} = 3.01$ T, $T2(t)$ and $T3(t)$ rise up first with $t(60\%) \simeq 1$ s, followed by $T1(t)$ and $T4(t)$ ($t(60\%) \simeq 2$ s) and $T0(t)$ rises up latest with $t(60\%) \simeq 3$ s. ΔT_{max} is larger for $T2$ and $T3$ ($\Delta T_{max} \simeq 12$ K) than for other points ($\Delta T_{max} \simeq 9$ K). In figure 2(*d*), $B_T{}^{3\,mm}$ for $B_{ex} = 3.01$ T is larger for points P2 ($B_T{}^{3\,mm}\,2 \simeq 0.70$ T) and P3 ($B_T{}^{3\,mm}\,3 \simeq 0.75$ T), while $B_T{}^{3\,mm}\,1$ and $B_T{}^{3\,mm}\,4$ are quite small. It is to be noted that $B_T{}^{3\,mm}\,0$ ($\simeq$0.4 T) is pretty large. The behaviour of $B_T{}^{3\,mm}$ suggests that the surface barrier against the flux penetration has been destroyed in GSR2 and GSR3 for $B_{ex} = 3.01$ T, while the barriers are kept intact in GSR1 and GSR4. The flux penetrates into the bulk along the paths such as circumference C–P2–P0 and C–P3–P0. The rapid and large rise of $T2$ and $T3$ means that the powerful heat source is located near P2 and P3. Especially, the characteristic $T3(t)$ behaviour with a sharp peak implies the heat generation in the very vicinity of P3. Since the flux motion necessarily generates heat inside the bulk through both the pinning power loss P_p and the viscous flow loss P_v,

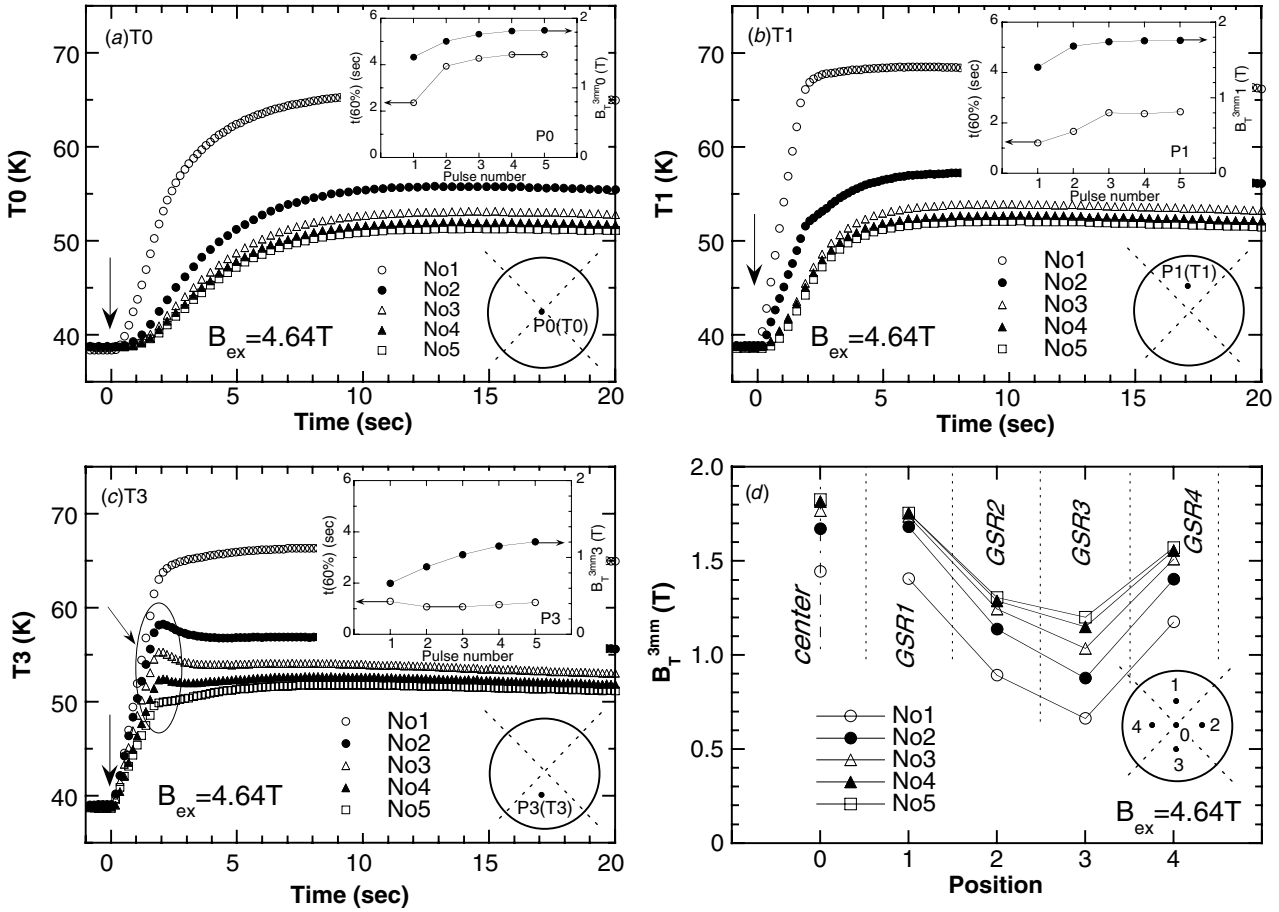

Figure 3. The time evolution of (*a*) *T*0, (*b*) *T*1 and (*c*) *T*3 after applying five repeated pulses of 4.64 T. The ellipse in (*c*) indicates the shoulder-like anomalies. The insets of each figure present the pulse number dependences of $t(60\%)$ and $B_{\mathrm{T}}{}^{3\,\mathrm{mm}}$ at respective positions. (*d*) The position and pulse number dependences of $B_{\mathrm{T}}{}^{3\,\mathrm{mm}}$ for $B_{\mathrm{ex}} = 4.64$ T pulses.

such a rapid rise of *T*2 and *T*3 suggests the existence of the easy path for the flux motion along C–P2–P0 and C–P3–P0. The formation of the easy paths may originate from relatively weaker pinning force F_{p} of GSR2 and GSR3. Even in the case of the flux penetration, *T*0(*t*) at the centre of the bulk rises up latest because the main heat generation still takes place in the peripheral region where the flux moves faster.

In figure 2(*c*) for $B_{\mathrm{ex}} = 3.87$ T, the position dependences of ΔT_{max} and $t(60\%)$ become smaller. The $t(60\%)$ values for *T*1–*T*4 are about 1 s and that of *T*0 is about 2 s. The time profiles of *T*1–*T*4 suggest that the surface barriers against the flux penetration have been destroyed in all the GSRs for $B_{\mathrm{ex}} = 3.87$ T. The rapid rises of *T*1–*T*4 mean that the flux penetrates pretty uniformly through the surfaces of the circumference of the four GSRs and heat is mainly generated in the peripheral regions inside the bulk. In figure 2(*d*), $B_{\mathrm{T}}{}^{3\,\mathrm{mm}}1$ and $B_{\mathrm{T}}{}^{3\,\mathrm{mm}}4$ for $B_{\mathrm{ex}} = 3.87$ T are larger than $B_{\mathrm{T}}{}^{3\,\mathrm{mm}}2$ and $B_{\mathrm{T}}{}^{3\,\mathrm{mm}}3$, contrary to the case of $B_{\mathrm{ex}} = 3.01$ T. Especially $B_{\mathrm{T}}{}^{3\,\mathrm{mm}}3$ values are almost the same for $B_{\mathrm{ex}} = 3.87$ T and $B_{\mathrm{ex}} = 3.01$ T. This fact indicates that a large amount of flux, which has penetrated during the increasing cycle of the pulse field, has also gone out of the bulk during the decreasing cycle along P0–P2–C and P0–P3–C easy paths.

Figure 2(*e*) presents $\Delta T0_{\mathrm{max}}$ and the trapped magnetic field $B_{\mathrm{T}}{}^{P}$ monitored by the Hall sensor fixed at PH as a function of B_{ex} (note that P0 is the nearest to PH). $\Delta T0_{\mathrm{max}}$ increases with increasing B_{ex} almost linearly. $B_{\mathrm{T}}{}^{P}$ suddenly increases for $B_{\mathrm{ex}} = 3.87$ T, takes a maximum for $B_{\mathrm{ex}} = 4.64$ T, and decreases with further increase of B_{ex}. The origin of the $B_{\mathrm{T}}{}^{P}$ decrease will be discussed later.

Figures 3(*a*)–(*c*) show the time evolution of *T*0, *T*1 and *T*3 after applying five repeated pulses of 4.64 T, respectively. The insets of each figure present the pulse number dependences of $t(60\%)$ and $B_{\mathrm{T}}{}^{3\,\mathrm{mm}}$ at respective positions. Figure 3(*d*) summarizes the position and pulse number dependences of $B_{\mathrm{T}}{}^{3\,\mathrm{mm}}$ for $B_{\mathrm{ex}} = 4.64$ T pulses. In figures 3(*a*)–(*c*), ΔT are the largest for the first (no 1) pulse and decrease with increasing pulse number, approaching a fixed ultimate behaviour for the nos 4 and 5 pulses. This behaviour is quite reasonable because the largest amount of the flux penetrates into the virgin state bulk during the no 1 pulse and the further flux penetration for the no 2 and succeeding nos 3–5 pulses should be limited because of the presence of the already trapped flux. Then the flux overall velocity is reduced, resulting in the reduction of the heat generation due to the flux motion. If $B_{\mathrm{T}}{}^{P}$ tends to saturate, the reduction of $\Delta T(t)$ is to equally saturate. A clear position dependence of $T(t)$ and the trapped field must not be overlooked. In the inset of figure 3(*b*), a saturation behaviour of $B_{\mathrm{T}}{}^{3\,\mathrm{mm}}1$ can be confirmed for the no 2 and following pulses. The rise time $t(60\%)$ of *T*1 is ∼1.2 s for the no 1 pulse, ∼1.6 s for no 2 and saturates at ∼2.4 s for the

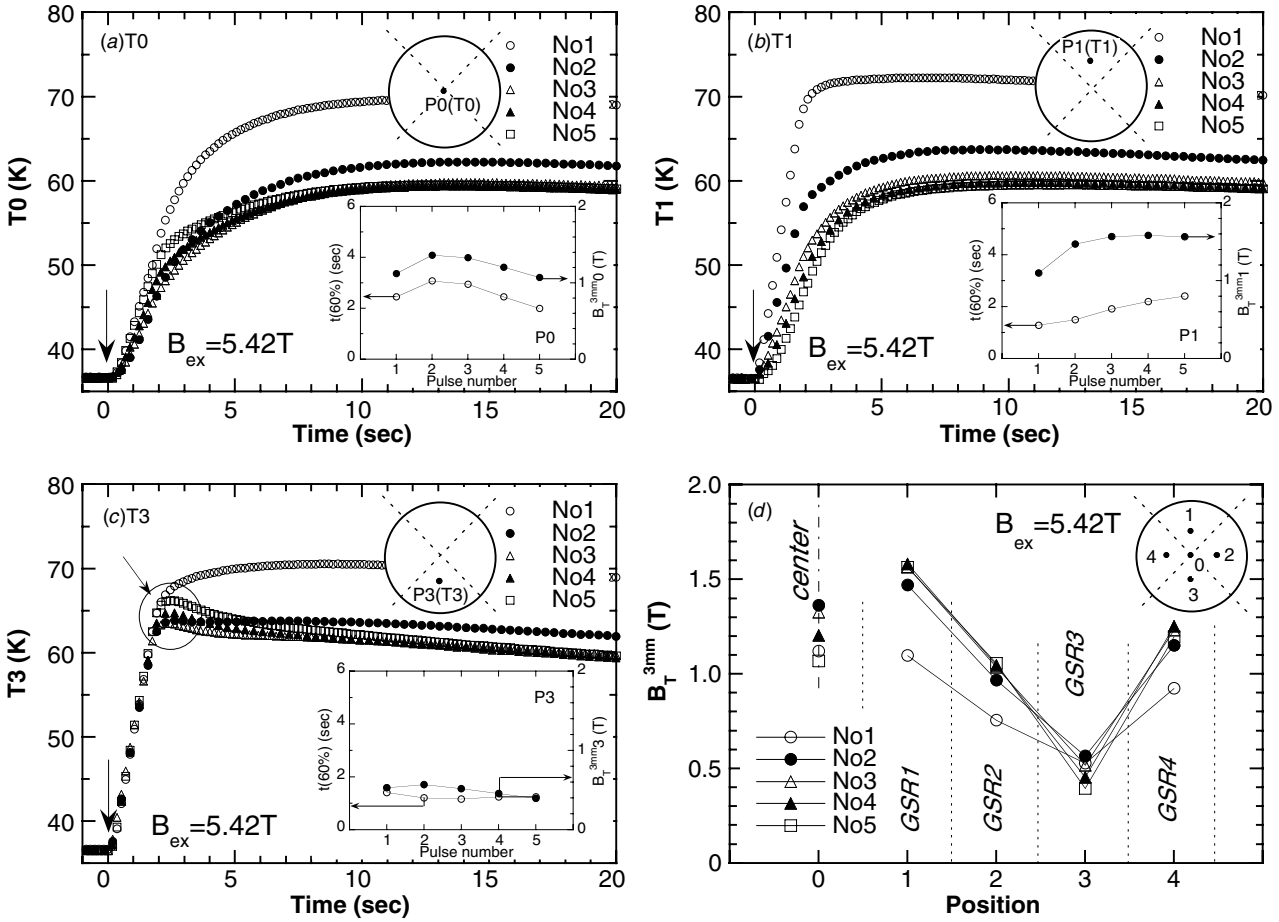

Figure 4. The time evolution of (*a*) $T0(t)$, (*b*) $T1(t)$ and (*c*) $T3(t)$ after applying five repeated pulses of 5.42 T. The circle in (*c*) indicates the shoulder-like anomalies. The insets of each figure present the pulse number dependence of $t(60\%)$ and $B_{\mathrm{T}}{}^{3\,\mathrm{mm}}$ at respective positions. (*d*) The position and pulse number dependences $B_{\mathrm{T}}{}^{3\,\mathrm{mm}}$ for $B_{\mathrm{ex}} = 5.42$ T pulses.

nos 3–5 pulses. These results indicate that the heat generation occurs mostly at peripheral region in the C–P1–P0 path after the no 3 and following pulses because the flux motion is small in the vicinity of P1 owing to the saturated $B_{\mathrm{T}}{}^{3\,\mathrm{mm}}1$. In contrast, the $B_{\mathrm{T}}{}^{3\,\mathrm{mm}}3$ values in the inset of figure 3(*c*) are relatively small and continue to increase gradually for the nos 3–5 pulses without showing the saturation behaviour. It is to be noted that $B_{\mathrm{T}}{}^{3\,\mathrm{mm}}3$ ($\simeq$0.65 T) after the no 1 pulse of $B_{\mathrm{ex}} = 4.64$ T is even smaller than the corresponding $B_{\mathrm{T}}{}^{3\,\mathrm{mm}}$ values for $B_{\mathrm{ex}} = 3.01$ T and 3.87 T. The $t(60\%)$ values of $T3$ are almost independent of the pulse number and remains at nearly a constant value ($\sim$1.2 s). The small and constant values of $t(60\%)$ of $T3$ suggest that the heat generation always takes place not only in the peripheral region but also in the vicinity of P3. This fact indicates that the flux motion along the C–P3–P0 path is also intense even for the nos 2–5 pulses. The unsaturating $B_{\mathrm{T}}{}^{3\,\mathrm{mm}}3$ may be correlated with the intense flux motion around P3 for every sequential pulse. In the inset of figure 3(*a*), $t(60\%)$ of $T0$ measured at the centre of the bulk is about $\sim$2.3 s for the no 1 pulse and then sharply increases to about 4 s for the no 2 and succeeding pulses. This result suggests that the flux motion near the central region occurs only for the no 1 pulse. In figure 3(*b*), $T1(t)$ shows a smooth variation on time for each pulse, while the characteristic peak again appears in $T3(t)$ for the nos 2–4 pulses, supporting the violent flux motion along the C–P3–P0 path. In figure 3(*d*), we can clearly see that the trapped field $B_{\mathrm{T}}{}^{3\,\mathrm{mm}}$ is the largest for the GSR1 and the smallest for the GSR3. This is consistent with the hard C–P1–P0 path and the easy C–P3–P0 path for the flux motion. The GSR2 provides the second easy path and the GSR4 provides the second hard path for the flux motion.

For higher pulse fields, the behaviour of $\Delta T(t)$ and $B_{\mathrm{T}}{}^{3\,\mathrm{mm}}$ remarkably changes. Figures 4(*a*)–(*c*) show $T0(t)$, $T1(t)$ and $T3(t)$ after applying the five sequential pulses of 5.42 T. The insets of each figure present the pulse number dependence of $t(60\%)$ and $B_{\mathrm{T}}{}^{3\,\mathrm{mm}}$ at respective positions. Figure 4(*d*) summarizes the position and pulse number dependences $B_{\mathrm{T}}{}^{3\,\mathrm{mm}}$ for $B_{\mathrm{ex}} = 5.42$ T pulses. In these figures, somewhat anomalous time evolutions of $T(t)$ and pulse number dependences of $t(60\%)$ and $B_{\mathrm{T}}{}^{3\,\mathrm{mm}}$ are observable at positions P0 and P3. In figure 4(*a*), $B_{\mathrm{T}}{}^{3\,\mathrm{mm}}0$ is the largest ($\sim$1.3 T) for the no 2 pulse and decreases for the following pulses. This is a clear sign that $B_{\mathrm{ex}} = 5.42$ T is too large to efficiently magnetize the present Sm-based bulk. The temperature rise due to rampant flux motion weakens F_{p} and hinders the field trapping at this high level of B_{ex}. In the inset, $t(60\%)$ of $T0$ also takes a maximum for the no 2 pulse and decreases for the following pulses. The short $t(60\%)$ of $T0$ suggests that the flux motion in the neighbourhood of the centre is enhanced for the nos 3–5 pulses, possibly reflecting the escape of the flux

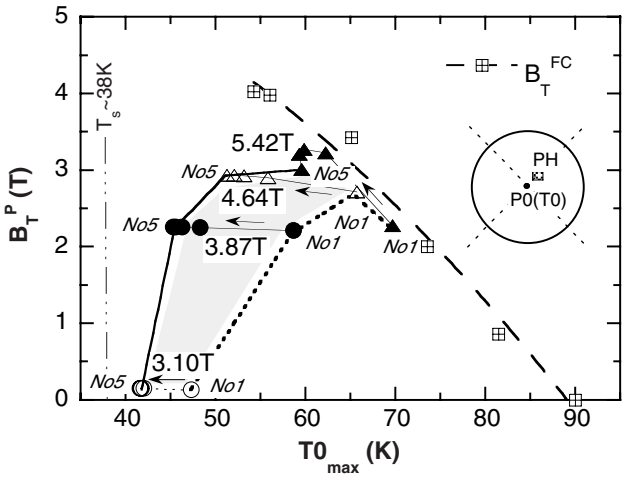

Figure 5. The summary of the trapped field $B_T{}^P$ versus the maximum temperature $T0_{max}$. The measured trapped field $B_T{}^{FC}$ by FCM corresponding to $T0_{max}$ is also presented.

from this region of the bulk. The similar anomalous behaviour can be seen for $B_T{}^{3\,mm}\,3$ and $t(60\%)$ in the inset of figure 3(*c*). On the other hand, $T1(t)$ shows a smooth time evolution and a smooth pulse number dependence. $B_T{}^{3\,mm}\,1$ and $t(60\%)$ of $T1$ in figure 3(*b*) also exhibit the normal behaviour similar to the case of $B_{ex} = 4.64$ T pulse; $B_T{}^{3\,mm}\,1$ saturates after the no 2 pulse and $t(60\%)$ gradually increases, showing a tendency for saturation. In figure 4(*d*), we note that the $B_T{}^{3\,mm}$ values are pretty smaller at every measuring point in comparison to $B_{ex} = 4.64$ T pulses. We also note that the pulse number dependences of $B_T{}^{3\,mm}\,0$ and $B_T{}^{3\,mm}\,3$ are much similar and decrease with the pulse number. This result strongly supports that the magnetic fluxes leave the central region mainly through the easy P0–P3–C path in GSR3.

Figure 5 shows the summary of the trapped field $B_T{}^P$ at PH versus the maximum temperature $T0_{max}$ at P0. The measured trapped field $B_T{}^{FC}$ by FCM corresponding to the temperature $T0_{max}$ is also presented in the figure. The temperature rise $\Delta T0^{FC}$ was monitored during the FCM operation, which was 4.2 K at $T0_{max} = 54$ K and decreased with increasing temperature. For $B_{ex} \leqslant 4.64$ T, the data set of $(B_T{}^P, T0_{max})$ is situated below the $B_T{}^{FC}$–$T0_{max}$ line for the no 1 pulse. For the succeeding pulses, $T0_{max}$ monotonically decreases and saturates. For $B_{ex} = 5.42$ T, on the other hand, $T0_{max}$ touches the $B_T{}^{FC}$–$T0_{max}$ line owing to the large temperature rise ($T0_{max} \simeq 70$ K) for the no 1 pulse and $B_T{}^P$ decreases following the $B_T{}^{FC}$–$T0_{max}$ line. As a result, $B_T{}^P$ for the no 1 pulse of 5.42 T is smaller than that for 4.64 T. For the no 2 pulse of 5.42 T, $B_T{}^P$ increases to the observed highest value of 3.22 T also nearly following this line because of the decreased $T0_{max}$. These analyses demonstrate that the flux trapping ability by the PFM technique can be systematically explained as limited by the $B_T{}^{FC}$–$T0_{max}$ line. The slight decrease of $B_T{}^P$ for the nos 4 and 5 pulses of 5.42 T may possibly be caused by the flux leaking out through the easy path in the GSR3 as mentioned above.

Finally, we comment on the possibility of the $B_T{}^P$ enhancement by the PFM method from the viewpoint of the temperature rise. First of all, starting with the initial temperature $T_s = 38$ K, the pulse fields smaller than ~2.5 T are useless because of the presence of the surface barrier against the flux intrusion. The main strategy to realize the largest $B_T{}^P$ is how to approach $B_T{}^{FC}$–$T0_{max}$ line without touching it. In figure 5, a series of data points for the nos 1 and 5 pulses are connected by the dotted and solid lines, respectively. The region left side of the solid line corresponds to the inevitable temperature rise region, which we cannot utilize by the present PFM apparatus. The hatched region surrounded by the dotted, $B_T{}^{FC}$–$T0_{max}$, and solid lines is the stage, on which the actual PFM process takes place. As for the no 1 pulse, $B_{ex} = 5.42$ T is too large because of too large ΔT. $B_{ex} = 4.64$ T for the no 1 pulse seems to be nearly the best choice and succeeding pulses with slightly larger B_{ex} may enhance the $B_T{}^P$. But it should be noted that the no 2 pulse of $B_{ex} = 5.42$ T have realized almost the possible extreme value of $B_T{}^P$. Although final pulse smaller than $B_{ex} \leqslant 4.64$ T may be effective to locally supplement the flux flowing out through the weaker pinning path (e.g., P0–P3–C), there seems to be only a little room for the $B_T{}^P$ enhancement with $T_s = 38$ K.

One possible scheme to overcome this difficulty is to make T_s lower. The maximum temperature of the bulk is expected to decrease with decreasing T_s for the same input heat generation. However, the effect is supposed to be small, even if T_s decreases down to 10 K, because the specific heat of the bulk becomes smaller and the cooling power of the GM refrigerator becomes lower in the lower temperature region. The second possible scheme may be to enhance the heat exhaust from the bulk. The dispersion of the Ag metal particles in the bulk to enhance the thermal conductivity and the specific heat is a possible method. The metal ring fitting tightly to the bulk disk may be effective in the efficient heat exhaust to the cold stage. If the temperature rise can be eliminated by increasing the heat exhaust against the same heat generation, $B_T{}^P$ may be improved even with the same initial temperature T_s.

4. Summary

The time evolution and position dependence of the temperature rise $\Delta T(t)$ after the five iterative pulse fields (nos 1–5) with the same amplitude have been measured on the surface of the four growth sector regions (GSR1–4) and of the centre (P0) of a cryo-cooled SmBaCuO bulk superconductor. The strength of the pulse field B_{ex} was varied between 2.32 T and 5.42 T and the initial temperature was set at $T_s = 38$ K. Important experimental results and conclusions obtained in this study are summarized as follows:

(1) For the no 1 pulse application, the trapped magnetic field $B_T{}^{3\,mm}$ monitored at 3 mm above the bulk surface is very small for $B_{ex} = 2.32$ T and the time constant of the temperature rise $t(60\%)$ is long ($\geqslant$2 s) for all GSRs. The results indicate the presence of the surface barrier against the flux intrusion and the heat generation due to the pulse application takes place just on the circumference of the bulk sample.

(2) The surface barrier is destroyed by $B_{ex} = 3.01$ T pulse for GSR2 and GSR3 and by $B_{ex} = 3.87$ T pulse for GSR1 and GSR4. The $t(60\%)$ values for the no 1 pulse become short (~1 s) in GSRs with destroyed barrier.

(3) In GSR3, there is a special path along which the magnetic flux moves through preferentially. The flux pinning force F_p may be relatively small in GSR3.
(4) For $B_{ex} \leqslant 4.64$ T, the temperature rise $\Delta T(t)$ is the largest for the no 1 pulse and decreases for the succeeding pulses. The increase of the trapped field ${B_T}^P$ is also the largest for the no 1 pulse, followed by a gradual increase for the nos 2 and 3 pulses. ${B_T}^P$ saturates for the nos 4 and 5 pulses. The behaviours of $\Delta T(t)$ and ${B_T}^P$ are stable for $B_{ex} \leqslant 4.64$ T. The rise time $t(60\%)$ is the shortest for the no 1 pulse and gradually increases with increasing pulse number, which suggests that the heat generation due to flux motion becomes limited in the peripheral regions for the succeeding pulses.
(5) For $B_{ex} = 5.42$ T, ${B_T}^P$, which is smaller than that for $B_{ex} = 4.64$ T after the no 1 pulse, takes a maximum for the no 2 or 3 pulse and decreases for the nos 4 and 5 pulses. $t(60\%)$ at the centre of the bulk sample also shows an unstable behaviour for the sequential pulse applications, taking a maximum for the no 2 pulse.
(6) The behaviour of ${B_T}^P$ can be understood on the basis of the diagram of the trapped field B_T versus the maximum temperature $T0_{max}$ at the centre. For $B_{ex} \leqslant 4.64$ T, the data set $({B_T}^P, T0_{max})$ does not touch the ${B_T}^{FC}$–$T0_{max}$ line for the flux trapping by the field cooled magnetizing. On the other hand, $({B_T}^P, T0_{max})$ touches the ${B_T}^{FC}$–$T0_{max}$ line for $B_{ex} = 5.42$ T due to too large ΔT after the no 1 pulse, resulting in the smaller ${B_T}^P$ than that for $B_{ex} = 4.64$ T. The touch to the ${B_T}^{FC}$–$T0_{max}$ line is the origin of the unstable behaviours of B_T^P and $t(60\%)$ in the iterative pulse field magnetizing process.

Acknowledgments

The valuable suggestions by professor M Ikebe of Iwate University are greatly acknowledged. This work is partially supported by Japan Science and Technology Corporation under the Joint-research Project for Regional Intensive in the Iwate Prefecture on Development of practical applications of magnetic field technology for use in the region and in everyday living.

References

[1] Murakami M, Sakai N, Higuchi T and Yoo S I 1996 *Supercond. Sci. Technol.* **9** 1015
[2] Mizutani U, Oka T, Itoh Y, Yanagi Y, Yoshikawa M and Ikuta H 1998 *Appl. Supercond.* **6** 235
[3] Ikuta H, Yanagi Y, Yoshikawa M, Itoh Y, Oka T and Mizutani U 2001 *Physica* C **357–360** 837
[4] Ishihara H, Ikuta H, Itoh Y, Yanagi Y, Yoshikawa M, Oka T and Mizutani U 2001 *Physica* C **357–360** 763
[5] Yanagi Y, Itoh Y, Yoshikawa M, Oka T, Yamada Y and Mizutani U 1997 *Advances in Superconductivity IX* (Tokyo: Springer) p 733
[6] Fujishiro H, Oka T, Yokoyama K and Noto K 2003 *Supercond. Sci. Technol.* **16** 809
[7] Kohayashi S and Nagaya S 2001 *Physica* C **357–360** 789
[8] Fujishiro H and Kohayashi S 2002 *IEEE Trans. Appl. Supercond.* **12** 1124